Isı Bilimi ve Tekniği Dergisi, 40, 1, 113-129, 2020
J. of Thermal Science and Technology

ISSN 1300-3615

A NOVEL THERMAL ANALYSIS FOR COOKING PROCESS IN BULGUR PRODUCTION: DESIGN CONSIDERATIONS, ENERGY EFFICIENCY AND WASTEWATER DIMINUTION FOR INDUSTRIAL PROCESSES

İbrahim Halil YILMAZ[*] and Mehmet Sait SÖYLEMEZ[**]
[*]Department of Mechanical Engineering, Adana Alparslan Türkeş Science and Technology University, Adana, iyilmaz@atu.edu.tr
[**]Department of Mechanical Engineering, Gaziantep University,Gaziantep, sait@gantep.edu.tr

(Geliş Tarihi: 24.07.2019, Kabul Tarihi: 24.02.2020)

Abstract: The main contribution of this study is to present a novel thermal model for analyzing the wheat cooking process and to propose a design procedure for an energy-efficient cooking pot. A small-scale cooking pot was designed and an experimental setup was installed to verify the model under various operating conditions. The developed model was solved using the Engineering Equation Solver software. Results were compared with those of the experiments and good agreement was obtained. Additionally, a computational fluid dynamics model was developed to verify the thermal model and have a useful design tool for large-scale cooking pots. It was found that the energy efficiency of the cooking process can be enhanced by initiating nucleate boiling (at ~5 °C minimum temperature difference between the heating element surface and saturation) which will supply the minimum heat flux on the helicoidal heat exchanger of the cooking pot. Lessening the energy demand but preserving the final product quality has decreased the 5-day biological oxygen demand of wastewater at least 50%. It is proposed that the wheat to water ratio can be reduced to 1.0−1.2 once the energy optimization and water recovery practices are satisfied. The estimated average specific energy consumption rate lies between 400–475 ±5% W/kg (thermal power supplied for one kilogram of wheat) which can be reduced ~25% further by reducing the wheat to water ratio to 1.0. The results reported in the present study are expected to guide thermal and food engineers for the design applications of industrial cooking pots, energy optimization with less harmful wastewater and process control strategies for cooking of wheat.
Keywords: Wheat cooking; bulgur; cooking model; energy analysis; cooker design; wastewater

BULGUR ÜRETİMİNDE PİŞİRME İŞLEMİNE YÖNELİK ÖZGÜN BİR ISIL ANALİZİ: ENDÜSTRİYEL SÜREÇLER İÇİN TASARIM ÖNERİLERİ, ENERJİ VERİMLİLİĞİ VE ATIKSU AZALTIMI

Özet: Bu çalışmanın ana katkısı, buğday pişirme işlemini özgün bir ısıl modelle izah ederek sunmak ve enerji-verimli bir pişirme kazanı için tasarım yöntemi önermektir. Küçük-ölçekli bir pişirme kazanı tasarlanmış ve modelin çeşitli çalışma şartları altında doğrulanması için bir deney düzeneği kurulmuştur. Geliştirilen model Engineering Equation Solver yazılımı kullanılarak çözülmüştür. Sonuçlar deneylerle kıyaslanmış ve iyi bir uyum elde edilmiştir. Isıl modelin doğrulanması ve büyük-ölçekli pişirme kazanlarına yönelik kullanışlı bir tasarım aracı olması için ayrıca bir hesaplamalı akışkanlar dinamiği modeli geliştirilmiştir. Pişirme işleminin enerji verimliliğinin, pişirme kazanının sarmal ısı değiştiricisi üzerindeki minimum ısı akısının çekirdekli kaynamayı (ısıtma elemanı yüzeyi ve doyma sıcaklığı arasında minimum ~5 °C farkla) karşılayacak şekilde başlatılmasıyla arttırılabileceği bulunmuştur. Enerji talebini azaltarak fakat nihai ürün kalitesini koruyarak, atıksuyun 5-günlük biyolojik oksijen ihtiyacı en az %50 oranında azaltılmıştır. Enerji optimizasyonu ve su geri kazanımı teknikleri yerine getirildiği takdirde buğday-su oranının 1,0−1,2'ye düşürülebileceği önerilmektedir. Tahmini ortalama özgül enerji tüketim hızının 400–475 ±%5 W/kg (bir kilogram buğday için gerekli olan ısıl güç) arasında yer almakta, bu değer buğday-su oranının 1,0'a düşürülmesiyle ilaveten ~%25 oranında azaltılabilmektedir. Çalışmadan elde edilen sonuçların ısı ve gıda mühendisleri için endüstriyel pişirme kazanlarının tasarım uygulamalarında, daha az zararlı atıksu ile enerji optimizasyonunda ve buğdayın pişirilmesi için süreç kontrol stratejilerinde kılavuzluk edeceği düşünülmektedir.
Anahtar Kelimeler: Buğday pişirme; bulgur; pişirme modeli; enerji analizi; kazan tasarımı; atıksu

NOMENCLATURE

a	radius of the coiled pipe [m]
A	cross-sectional area [m^2]
b	coil pitch [m]
BOD_5	5-day biological oxygen demand [mg/L]
c_p	specific heat capacity [J/kg°C]
D	diameter [m]; diffusion coefficient [m^2/s]
De	Dean number [$= \mathrm{Re}\left(a/R\right)^{1/2}$]
g	gravitational acceleration [m/s^2]
Gr	Grashof number [$= g\left(\rho_s - \rho_\infty\right)L_c^3/\rho\nu^2$]
h	convective heat transfer coefficient [$W/m^2°C$]
H	height [m]
He	Helical number [$= \mathrm{De}\left(1+\left(b/2\pi R\right)^2\right)^{1/2}$]
h_{fg}	enthalpy of vaporization [J/kg]
k	thermal conductivity [W/m°C]
L_c	characteristic length [m]
m	mass [kg]
$\dot{m}$	mass flowrate [kg/s]
M_w	molecular weight of water [kg/mol]
Nu	Nusselt number [= hD/k]
P	pressure [Pa]
Pr	Prandtl number [$= \mu c_p/k$]
$\dot{q}$	heat flux [W/m^2]
Q	heat transfer [J]
$\dot{Q}$	heat transfer rate [W]
R	coil radius [m]; universal gas const. [J/K mol]
Ra	Rayleigh number [$= g\beta\left(T_s - T_\infty\right)L_c^3\,\mathrm{Pr}/\nu^2$]
Re	Reynolds number [= $u_m D/\nu$]
Sh	Sherwood number [$Sh = hL_c/D$]
t	thickness [m]; time [s]
T	temperature [°C]
u_m	mean velocity [m/s]
U	overall heat transfer coefficient [$W/m^2°C$]
W	moisture content [%]
x_a	air mass fraction [$= m_{air}/\left(m_{air}+m_v\right)$]

Greek letters

α	inclination angle [°]
ΔT_{excess}	excess temperature [°C]
μ	dynamic viscosity [kg/m·s]
ν	kinematic viscosity [m^2/s]
ρ	density [kg/m^3]
σ	surface tension [N/m]
ϕ	relative humidity [$= P_v/P_g$]

Subscripts

a	absorbed
air	air
ave	average
b	boiling
bulk	bulk fluid
c	critical; condensation
cp	cooking pot
d	dry basis
e	equivalent water of metallic parts
ev	evaporated water
f	film; flash
g	grain; gas
htf	heat transfer fluid
i	inner
in	inlet
ins	insulation
m	mixture
l	liquid
loss	loss
o	outer
out	outlet
p	pipe; preheating
r	residual
s	surface; sensible
sat	saturation
v	vapor
w	water; wall

Abbreviations

CFD	computational fluid dynamics
CHE	coiled heat exchanger
CP	cooking pot
EES	Engineering Equation Solver
GP	gear pump
HTF	heat transfer fluid
ONB	onset of nucleate boiling
TCEH	temperature controlled electric heater
TET	thermal expansion tank
WPT	water preheating tank

INTRODUCTION

Cooking is the initial step for the production of certain cereal products. Typically, grains are heated firstly with water at elevated temperatures and pressures in this process. After cooking, the grains become soft enough to be worked into the final product. During this process, it is essential to obtain a product at the desired quality and the lowest cost since it requires a significant amount of thermal energy. The cooking process of cereal products involves both the diffusion of water into grains and the subsequent conversion (reaction) of starch within them i.e., gelatinization. The literature on the cooking model of wheat is limited and largely focused on the effects of cooking time, temperature and starch gelatinization. Stapley *et al.* (1998) studied the diffusion and reaction behaviors of wheat grains during boiling. They developed a diffusion model using the finite-element method and tested certain model scenarios to compare the simulation results with the experimental data for moisture distribution across the central section of grains at 100 °C and 120 °C. Watanabe *et al.* (2001) proposed a new mathematical model to describe the moisture profile in starchy food during cooking. Bayram (2005) determined the cooking degree of wheat kernels by using three different gelatinization measuring methods. The optimum cooking time was specified to be 40 min at 97 °C in case of maintaining 100% gelatinization without

any deformation on wheat kernels. Lately, Balcı and Bayram (2020) investigated the possibility of cooking wastewater reuse for the subsequent cooking operation obtained from the former process. It was indicated that the energy requirement might be reduced by 57% at the expense of increasing 5-day biological oxygen demand (BOD_5) and filtering cost.

Physically, cooking is a type of thermal process which involves boiling that occurs at the solid-liquid interface when a liquid is brought into contact with the solid surface of heating material maintained at a temperature sufficiently above the saturation temperature of the liquid. Unlike ordinary cooking pot (CP), a pressure cooker is an appliance that is used to cook foods at high pressure and temperature to reduce the cooking time. The use of saturated steam and reduction in cooking time are the two methods of preserving vitamins (Rocca-Poliméni *et al.*, 2011). Pressure cookers have many nutritional, organoleptic and sanitary advantages however the literature does not have sufficient studies to explain these traits (Koca and Anıl, 1996; Rocca-Poliméni *et al.*, 2011). Rocca-Poliméni *et al.* (2011) developed a model which includes the physical and thermal characteristics of a commercial pressure cooker and of the food cooked in it based on the energy balance and heat and mass transfer relations.

In this study, the physical insight of cooking phenomena was described in detail and a novel thermal model was proposed for a small-scale industrial wheat CP. The developed model was coded in EES (Engineering Equation Solver) and the model results were compared with those of the experiments done. Additionally, a computational fluid dynamics (CFD) analysis was conducted to verify the thermal model and to present a design procedure for large-scale CPs. The prediction of specific energy demand for the cooking process was made by the methodology proposed for the first time. The wastewater properties after the cooking process were investigated to enhance energy efficiency and water recovery. As a result, a guide for the design applications of industrial CPs, energy optimization with less harmful wastewater and process control strategies for cooking of wheat has been presented.

DESCRIPTION OF COOKING MECHANISM

In industrial processes, process-water is firstly preheated to the temperature of 90 °C and then discharged into the CP. The temperature of the preheated water falls down when it is mixed with the unsoaked wheat grains (initially at about ambient temperature) inside the CP. After the discharging process, the mixture is heated up until the cooking temperature reaches the boiling temperature. The degree of cooking temperature is adjusted according to the condition of starch gelatinization since the degree of gelatinization of hard wheat starch depends strongly on cooking temperature. The rate of the gelatinization increases with increasing cooking temperature (Bakshi and Singh, 1980) and it is never completed 100% at a cooking temperature lower than 90 °C (Turhan and Gunasekaran, 2002). The amount of energy supply during the boiling process is regulated to keep the central region of the CP (charged with bulky wheat) at the cooking temperature.

THERMAL MODELING OF COOKING PROCESS

The detailed drawing of the CP used in the experimental setup is demonstrated in Figure 1. The CP was custom-designed (Yılmaz, 2018) and suited for industrial applications and its specifications are introduced in Table 1. A metal screen made of the perforated sheet was placed into the CP to prevent the direct contact between the wheat grains and the coiled pipe (i.e., coiled heat exchanger, CHE). Thus, the wheat grains will not adhere to the surface of the CHE whose temperature is high due to the heat transfer fluid (HTF) flowing inside it. The outer surface of the CP was well insulated to minimize the heat loss to the surroundings.

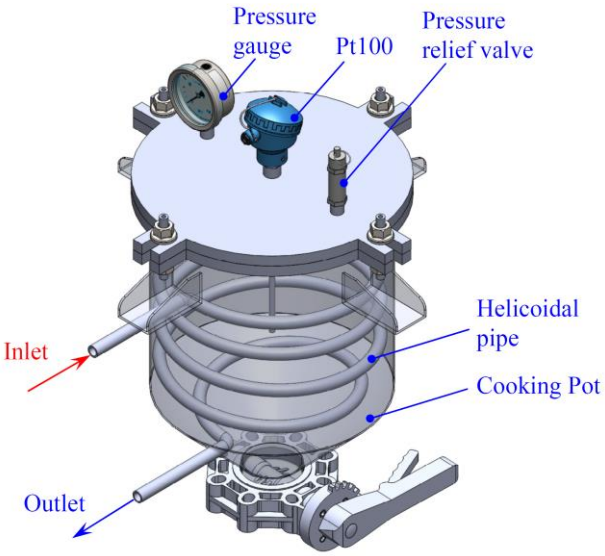

Figure 1. CP design used in the experimental setup.

Table 1. Specifications of the CP.

Sheet material	316L SS
Inner diameter of CP, $D_{i,cp}$	0.4 m
Material thickness of CP, t	0.002 m
CHE material	304L SS
CHE pipe diameter, $D_{i,p}/D_{o,p}$	0.0157/0.0213 m
Coil pitch, b	0.085 m
Coil radius, R	0.175 m
CHE effective surface area, A_s	0.288 m^2
Volume of CP	0.06 m^3
Insulated material	Stone wool

Heating Process of Water-grain Mixture (Sensible Heat Gain)

After the preheated water is discharged onto wheat grains, it is heated from the mixture temperature, T_m to the boiling temperature, T_b. This heating process is named as subcooled or local boiling since the main body

of the liquid temperature is below the saturation temperature, T_{sat}. At the early stages of boiling, the bubbles are confined to a narrow region near the hot surface. This is because the liquid adjacent to the hot surface vaporizes as a result of being heated above its saturation temperature. However, these bubbles disappear soon before reaching the liquid-gas interface as a result of heat transfer from the bubbles to the cooler liquid surrounding them. In this case, only sensible heat gain is considered for the heating process and the final temperature of the mixture can be calculated by using energy balance:

$$m_g c_{p,g}\left(T_m - T_g\right) = \left(m_w + m_e\right) c_{p,w}\left(T_w - T_m\right) \tag{1}$$

The sensible energy demand of the mixture to reach the boiling temperature can be defined by

$$Q_s = \left(m_w + m_e\right) c_{p,w}\left(T_b - T_m\right) + m_g c_{p,g}\left(T_b - T_m\right) \tag{2}$$

During the preheating process, some water will penetrate into the grains so that the amount of process-water will decrease and the moisture within the grains will increase with time. Thus, the specific heat of the grain samples will change through the temperature rise from T_m to T_b. The value of $c_{p,g}$ is estimated by the relation (Bruce and Giner, 1993):

$$c_{p,g} = c_{p,d} + c_{p,w} W \tag{3}$$

Mass transfer by evaporation

During the transition from subcooled boiling to saturated boiling, mass transfer by evaporation takes place at the liquid-gas interface as a result of water molecules diffusing into the air confined in the CP. This process continues until the phase equilibrium is maintained at boiling temperature since the vapor pressure at the mixing temperature is less than the saturation pressure of the liquid. The basic theory for estimating the evaporated water is presented in detail (Yılmaz, 2014).

$$\frac{dm_{ev}}{dt} = \frac{-A_{cp} D_{w-air}}{H_w - H_{cp}} \left(\frac{M_w P_v}{R\, T_v}\right)(1-\varphi) \tag{4}$$

Energy transfer to process-water

The constant mass flow inside the CHE is stated by forced circulation due to the pumping of the HTF (Yılmaz *et al.*, 2018). The dynamical state of the single-stream steady pipe flow shown in Figure 2 is determined by the flow parameter, Reynolds number (Re).

Curved or helicoidal pipes are widely used in engineering applications such as food processing. Contrary to straight pipes, the following dimensionless parameters are used in flow and heat transfer calculations of helicoidal pipes:

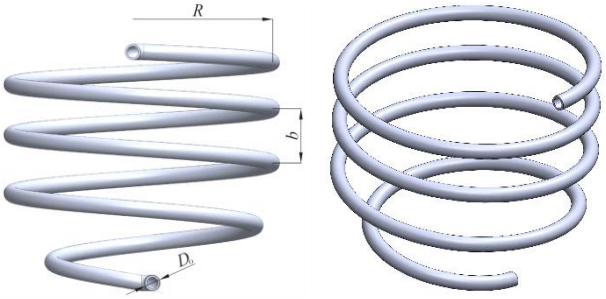

Figure 2. Geometry of the CHE.

$$\mathrm{De} = \mathrm{Re}\left(\frac{a}{R}\right)^{1/2} \tag{5}$$

$$\mathrm{He} = \mathrm{De}\left[1 + \left(\frac{b}{2\pi R}\right)^2\right]^{1/2} \tag{6}$$

$$R_c = R\left[1 + \left(\frac{b}{2\pi R}\right)\right] \tag{7}$$

where De is the Dean number, He is the Helical number, a denotes the radius of the circular pipe (i.e., $D_o/2$ in this study), b represents the coil pitch, R is the radius of the coil and the effective radius of curvature, R_c.

The estimation of the critical Re, which is used to identify the transition from the laminar to the turbulent regime in curved or helicoidal pipes, has been recommended by (Srinivasan *et al.*, 1970) for design purposes:

$$\mathrm{Re}_c = 2100\left[1 + 12\left(\frac{R}{a}\right)^{-0.5}\right] \tag{8}$$

The fully developed Nusselt number (Nu) relation for the laminar regime in helicoidal pipes subjected to uniform wall temperature was derived theoretically and experimentally by many researchers (Rohsenow *et al.*, 1998). For the corresponding thermal boundary condition, the Nu relation has been proposed by (Manlapaz and Churchill, 1981).

$$\mathrm{Nu}_i = \left[\left(3.657 + \frac{4.343}{\left(1 + \dfrac{957}{\mathrm{Pr}_{htf}\,\mathrm{De}^2}\right)^2}\right)^3 + 1.158\left(\frac{\mathrm{De}}{1 + \dfrac{0.477}{\mathrm{Pr}_{htf}}}\right)^{3/2}\right]^{1/3} \tag{9}$$

The flow inside the CHE shows turbulent behavior although the Re is close to the critical Re of the transitional regime. Hogg (1969) has indicated that

turbulent entrance length in coils with circular cross-sections much shorter than that of laminar flow. Turbulent flow can be fully developed within the first half-turn of the CHE. Therefore, most of the turbulent flow and heat transfer analyses concentrate on the fully developed region in CHEs. The fully developed Nu relation for turbulent flow in helicoidal pipes subjected to constant wall temperature was recommended by the Pratt (1947) equation which was modified by Orlov and Tselishchev (1964) for the influence of temperature-dependent properties as below:

$$\mathrm{Nu}_i = \mathrm{Nu}_p \left(1 + 3.54\frac{a}{R}\right)\left(\frac{\mathrm{Pr}_{bulk}}{\mathrm{Pr}_w}\right)^{0.25} \quad \begin{matrix} 5 < R/a < 84 \\ 1500 < \mathrm{Re} < 2\times10^4 \end{matrix} \tag{10}$$

where Nu_p is the Nusselt number for plain tubes which is estimated using the Dittus-Boelter equation (Çengel and Ghajar, 2011):

$$\mathrm{Nu}_p = 0.023\,\mathrm{Re}_{htf}^{0.8}\,\mathrm{Pr}_i^{0.3} \tag{11}$$

The convection heat transfer coefficient of the HTF is calculated using (Yılmaz and Söylemez, 2014)

$$h_i = \mathrm{Nu}_i \frac{k_{htf}}{D_{i,p}} \tag{12}$$

All fluid properties inside the pipe were evaluated at the bulk fluid temperature, i.e., $T_{bulk} = (T_{in} + T_{ex})/2$. The thermophysical properties of the HTF (Renolin therm 320 thermal oil) as a function of temperature were fitted to polynomial functions from the manufacturer's supplied data (Fuchs, 2013) as below:

$$\rho = 1058.108 - 0.6507T \tag{13}$$

$$c_p = 692.37 + 4.2887T \tag{14}$$

$$k = 0.15399 - 7.1764\times10^{-5}T \tag{15}$$

$$\mu = 0.3345 - 2.15348\times10^{-3}T + 4.66657\times10^{-6}T^2 - 3.39167\times10^{-9}T^3 \tag{16}$$

where ρ, c_p and k are valid in the temperature range of 273 K ≤ T < 473 K while μ is valid in 373 K ≤ T < 473 K. For any given temperature during iterations, Eqs. (13)−(16) were used without any problem.

Cooking Process of Mixture (Latent Heat Gain)

Transition from subcooled boiling to saturated boiling

Boiling is classified as pool boiling or flow boiling, depending on the presence of bulk fluid motion. It is called pool boiling in the absence of bulk fluid flow or called flow boiling (or forced convection boiling) in the presence of it. In this study, it is dealt with pool boiling rather than flow boiling. Four different boiling regimes are observed in pool boiling: natural convection, nucleate, transition and film boiling as illustrated in Figure 3. The specific shape of the curve depends on the fluid-heating surface material combination and the fluid pressure however it is practically independent of the geometry of the heating surface and its orientation (Çengel and Ghajar, 2011).

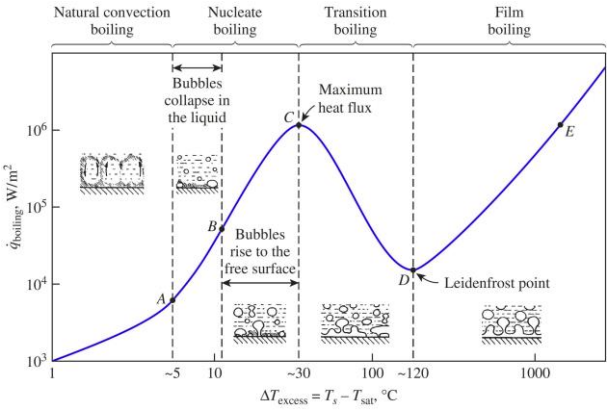

Figure 3. Typical boiling curve for water at 1 atm pressure. Adapted from (Çengel and Ghajar, 2011).

In the natural convection regime, the heat transfer takes place from the heater surface (only a few degrees above the saturation temperature i.e., towards point A or ONB (onset of nucleate boiling)) to the saturated liquid. The fluid motion in this mode of boiling is governed primarily by natural convection currents. If the temperature of the heating surface becomes higher than the saturation temperature, the regime is replaced from free convection to nucleate boiling. In the nucleate boiling regime, the bubbles start to form at various preferential sites on the heating surface. They are detached from the surface and dissipated in the liquid as receiving high heat fluxes. The nucleation sites form at an increasing rate so that the continuous columns of vapor appear as moved along the boiling curve from B to point C. As a result, very high heat fluxes are obtainable in this region. The nucleate boiling region ends and the unstable region (existence of partially both nucleate and film boiling) begins after the maximum (critical) is reached. As the heater temperature is increased past point C, the heat flux decreases as shown in Figure 3 since a large fraction of the heater surface is covered by a vapor layer which acts as an insulation due to its low thermal conductivity. Thus, operation in the transition boiling regime is generally avoided in practice when high temperatures involved. Nucleate boiling at point C is completely replaced by film boiling at point D. Beyond point D, the heater surface is completely covered by a continuous stable vapor layer. The presence of the vapor layer is responsible for the low heat transfer rates in the film boiling region. The heat transfer rate increases with increasing ΔT_{excess} as a result of heat transfer from the

heated surface to the liquid through the vapor film by radiation, which becomes significant at high temperatures.

Numerous experimental investigations have been reported in the literature for characterizing the heat transfer behavior in the nucleate boiling region (Cornwell and Houston, 1994). However, the derivation of heat transfer correlations for nucleate pool boiling is accompanied by difficulty (Rohsenow *et al.*, 1998). Any designer is faced with the problem of calculating the heat transfer coefficient for the nucleate boiling region where the use of correlations is inevitable although the designer should be aware of the uncertainties involved. Based on the problem physics, these correlations may yield different predictions for the estimation of the heat transfer coefficient. For nucleate pool boiling on horizontal tubes, the following correlation gives reasonable results (Cornwell and Houston, 1994):

$$\mathrm{Nu}_o = 9.7 P_c^{0.5} F'' \mathrm{Re}_b^{2/3} \mathrm{Pr}_b^{0.4} \tag{17}$$

where P_c is the critical pressure in bar and F'' is given by Eq. (17)

$$F'' = 1.8\left(P_{sat}/P_c\right)^{0.17} + 4\left(P_{sat}/P_c\right)^{1.2} + 10\left(P_{sat}/P_c\right)^{10} \tag{18}$$

Under saturated pool boiling conditions, the boiling Re becomes

$$\mathrm{Re}_b = \frac{\dot{q}_b D_{o,p}}{\mu_l h_{fg}} \tag{19}$$

Average heat transfer coefficient on the tube is defined as

$$h_o = \mathrm{Nu}_o \frac{k_w}{D_{o,p}} \tag{20}$$

Mass diffusion into wheat grains

The moisture content of wheat grains varies with time due to water diffusion until the wheat grains are not able to accept moisture uptake anymore. Absorbed water throughout the cooking process can be estimated by summing up water absorbed by wheat grains in both preheating and boiling processes.

$$m_a = m_g \frac{\left[\left(W_p - W_d\right) - \left(W_b - W_p\right)\right]}{100} \tag{21}$$

Condensation heat transfer

Water condensation takes place on the inner surfaces of the CP (cover plate and lateral wall) when the surface temperature falls below the dew point temperature of the evaporated water. Heat transfer rates for laminar film condensation on the horizontal and inclined downward-facing surfaces are predicted by assuming the condensate flow to be quasi-steady. This assumption makes it possible to determine the final shape of the liquid-vapor interface and thus to predict the average heat transfer coefficient. Gerstmann and Griffith (1967) studied the film condensation on the underside of horizontal and inclined surfaces. A slight inclination angles ($\alpha < 7.5°$), various wave patterns were observed. At moderate inclination angles ($\alpha > 20°$), roll waves appeared. The net effect of the roll waves increases and remains nearly constant up to 20° from the horizontal. However, the interfacial waves appear to be unchanged between 20°–90°.

For a horizontal surface, they developed the modified Rayleigh number (Ra_c) to estimate Nu:

$$\mathrm{Ra}_c = \frac{g\rho_l\left(\rho_l - \rho_g\right)h_{fg}}{\mu_l \Delta T k_l}\left(\frac{\sigma}{g\left(\rho_l - \rho_g\right)}\right)^{3/2} \tag{22}$$

The Nu relation for laminar film condensation is recommended to be

$$\mathrm{Nu}_c = \begin{cases} 0.69\mathrm{Ra}_c^{0.20} & 10^6 < \mathrm{Ra}_c < 10^8 \\ 0.81\mathrm{Ra}_c^{0.193} & 10^8 < \mathrm{Ra}_c < 10^{10} \end{cases} \tag{23}$$

For slightly inclined surfaces i.e., $\alpha < 20°$, Nu_c and Ra_c are modified in the above equations by replacing g by $g\cos\alpha$.

The presence of air (non-condensable gas) in the CP hinders the condensation heat transfer. Minkowycz and Sparrow (1966) investigated the effects of non-condensable gas, interfacial resistance, superheating, free convection, mass, and thermal diffusions and variable properties of liquid and gas-vapor regions on laminar film condensation. It was demonstrated that small concentrations of non-condensable gases can have a decisive effect on the heat transfer rate. Chin (1995) performed a numerical study for the influence of air-mass fraction ($x_a = m_{air}/(m_{air}+m_v)$) on condensation rate over a vertical plate with respect to stagnant or moving steam–air mixtures and compared their results with the experimental values obtained by Minkowycz and Sparrow (1966).

Figure 4 shows the agreement between these two models. The ratio between the condensation rate of the mixture and pure steam (K_{air}) depends mainly on x_a and slightly on the temperature difference between the gas and the wall. The variation of K_{air} obtained by (Chin, 1995) was proposed in order to predict the heat transfer coefficient due to condensation as a function of x_a for the temperature range of ($T_b - T_w$). Here, T_b is the boiling temperature and T_w is the wall temperature which will be estimated from the heat loss analysis of the CP.

Accordingly, the mass of condensed steam is predicted by

$$m_c = \frac{K_{air} h_c \left(T_b - T_w\right)}{h_{fg@T_b}} \tag{24}$$

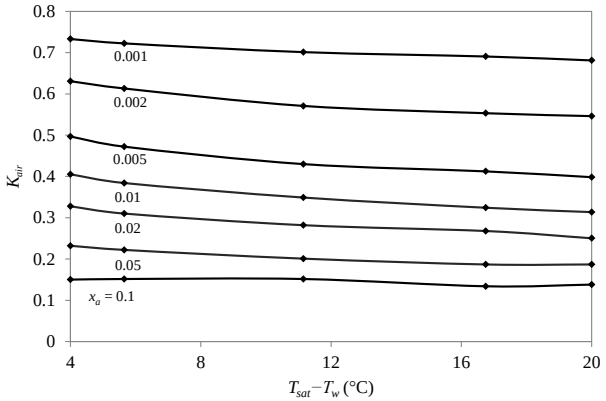

Figure 4. Condensation heat transfer in the presence of a non-condensable gas in quiescent mixture at T_{sat} = 100 °C. Adapted from (Chin, 1995).

Heat loss to surroundings

Heat loss from the outer surface of the CP (the lateral sides and cover plate) is estimated using the following relations:

For the lateral side in a cylindrical shape, the average Nu relation for an isothermal vertical plate can be evaluated using the relation proposed by (Churchill and Chu, 1975):

$$\mathrm{Nu}_{air} = \left\{ 0.825 + \frac{0.387\mathrm{Ra}_{air}^{1/6}}{\left[1+\left(0.492/\mathrm{Pr}_{air}\right)^{9/16}\right]^{8/27}} \right\}^2 \tag{25}$$

For the lateral side in a conical shape, Ra_{air} is modified in Eq. (25) replacing g by $g\cos\alpha$.

For the cover plate, the average Nu relation can be determined using power-law relations proposed by (Fujii and Imura, 1972) for horizontal surface facing upwards.

$$\mathrm{Nu}_{air} = \begin{cases} 0.16\mathrm{Ra}_{air}^{1/3} & 2\times10^8 < \mathrm{Ra}_{air} \\ 0.13\mathrm{Ra}_{air}^{1/3} & 5\times10^8 < \mathrm{Ra}_{air} \end{cases} \tag{26}$$

Noting that all fluid properties were evaluated at the film temperature, $T_f = (T_{s,cp} + T_{air})/2$.

Through the analysis of heat loss from the CP, the thermal resistance approach presented in (Çengel and Ghajar, 2011) was used where the heat flow from the boiling water to the ambient air combined into a single resistance $(UA)_{cp}$ as

$$\frac{1}{(UA)_{cp}} = \frac{1}{h_o A_{i,cp}} + \frac{\mathrm{In}\left(D_{o,cp}/D_{i,cp}\right)}{2\pi L k_{cp}} + \frac{\mathrm{In}\left(D_{o,ins}/D_{i,ins}\right)}{2\pi L k_{ins}} + \frac{1}{h_{air} A_{o,cp}} \tag{27}$$

The total heat loss from the CP is found to be

$$\dot{Q}_{loss} = (UA)_{cp}\left(T_b - T_{air}\right) \tag{28}$$

Mass transfer by flash evaporation

At the end of the cooking process, the energy transfer to the mixture is finished and the butterfly valve at the bottom side of the CP is opened for a while. The water in the CP evaporates due to flash boiling as a result of the concentration differences between the saturated water and ambient air. The diffusion of water vapor in the air was estimated by the empirical equations below (Marrero and Mason, 1972):

$$D_{w-air} = 1.87\times10^{-10}\frac{T^{2.072}}{P} \qquad 280\,\mathrm{K} < T < 450\,\mathrm{K} \tag{29}$$

Utilizing the analogy between heat and mass convection, the mass transfer coefficient is determined by

$$h_f = \frac{\mathrm{Sh}\, D_{w-air}}{L_c} \tag{30}$$

The Sherwood number (Sh) and the mass transfer coefficients were determined for the case of a horizontal surface:

$$\mathrm{Sh} = \begin{cases} 0.54\left(\mathrm{Gr\,Sc}\right)^{1/4} & 10^4 < \mathrm{Gr\,Sc} < 10^7 \\ 0.15\left(\mathrm{Gr\,Sc}\right)^{1/3} & 10^7 < \mathrm{Gr\,Sc} < 10^{11} \end{cases} \tag{31}$$

where $\mathrm{Gr} = g\left(\rho_s - \rho_\infty\right)L_c^3/\rho\nu^2$ and $Sc = \nu/D_{w-air}$ is the Schmidt number.

The evaporation heat transfer rate is estimated from

$$\dot{m}_f = h_f A_w\left(\rho_{v,s} - \rho_{v,\infty}\right) \tag{32}$$

Mass balance of water

During cooking operation, the total mass of water is conserved. This can be defined by the following equation:

$$m_t - \int_0^{\Delta t_1}\dot{m}_{ev}dt - \int_0^{\Delta t_2}\left(\dot{m}_b - \dot{m}_c\right)dt - \int_0^{\Delta t_3}\dot{m}_f dt - m_{loss} - \left(m_r - m_l\right) - m_a = 0 \tag{33}$$

where m_t is the total amount of process-water charged into the CP at the beginning of the cooking process, $\dot{m}_{ev}$ is the total evaporated water during Δt_1 (the preheating process of the water-wheat mixture), $\dot{m}_b - \dot{m}_c$ is the difference between the total amount of water boiled and condensed during Δt_2 (boiling process), $\dot{m}_f$ is the total amount of flashed water along Δt_3 (opening the cover plate to ambient air), m_{loss} is the flashing and evaporating water losses from the CP and bulgur respectively during

the depressurizing the CP with opening the butterfly valve, $m_r - m_l$ is the difference between the amount of residual water, m_r obtained at the end of cooking process and the leached substances, m_l existing in the residual water, m_a is the amount of water absorbed by wheat grains during cooking operation.

Cooking load

The outlet temperature of the HTF is estimated by using energy balance and the heat transfer equations derived in the previous sections. In this estimation, the radiation heat transfer among the lateral walls, food, and the CHE was considered negligible as compared to the condensation heat transfer since the surfaces have a low emissivity (stainless steel) and small temperature difference with their surroundings and the water vapor absorbs infrared radiation, as well. Only the energy supplied to the CP was taken into consideration to launch nucleate boiling and compensate for the heat loss.

As a form of convection heat transfer, the boiling heat flux from a solid surface to the fluid is expressed from Newton's law of cooling as

$$\dot{q}_b = h_o \Delta T_{excess} \tag{34}$$

where $\Delta T_{excess} = T_s - T_{sat}$ which represents the temperature excess of the surface above the saturation temperature of the fluid.

The energy transferred to the mixture during boiling can be written under the steady-state condition as

$$\begin{aligned} \dot{Q}_{cp} &= \dot{m}_{htf} c_{p,ave} \left(T_{in} - T_{ex}\right) \\ &= h_i A_s \Delta T_{lm} = \dot{q}_b A_s = \dot{m}_b h_{fg@T_b} \end{aligned} \tag{35}$$

where $\Delta T_{lm} = \dfrac{\Delta T_1 - \Delta T_2}{\ln\left(\Delta T_1 / \Delta T_2\right)}$ and here $\Delta T_1 = T_{h,in} - T_s$, $\Delta T_2 = T_{h,out} - T_s$, respectively.

The exit temperature of the HTF can be predicted by

$$T_{ex} = T_s + \left(T_s - T_{in}\right) e^{\frac{-h_i A_s}{\left(\dot{m} c_p\right)_{htf}}} \tag{36}$$

The governing equations were modeled in EES and solved simultaneously.

NUMERICAL ANALYSIS

CFD is a useful tool for simulating the flow field (Mwesigye *et al.*, 2018) and reproducing data during the design cycle (Yılmaz and Mwesigye, 2018). The design can be improved using this tool for optimization purposes. A CFD analysis was conducted to verify the thermal model and to extend it as a design procedure for large-scale CPs and improving the design by subsequent parametric analyses. For the numerical simulations, ANSYS Fluent v17.2 was used to solve the governing equations (the conservation equations for mass, momentum and energy) along with the boundary conditions applied. The flow inside the CHE was considered steady-state and fully developed turbulent. These considerations are reasonable since the experimental measurements were taken under steady conditions and the flow is fully developed due to the negligible entrance effect compared to the coil length.

Mesh Structure

The mesh structure of the CHE is shown in Figure 5. Mesh dependency studies were applied for each run considered in the study. The solution was considered grid-independent when the maximum changes in the outlet temperature were less than 1% based on the change of mesh element size. The numbers of mesh elements with 3,685,776; 7,100,622 and 11,217,391 were applied for mesh refinement, respectively however the 7,100,622 mesh element case was used in the analyses.

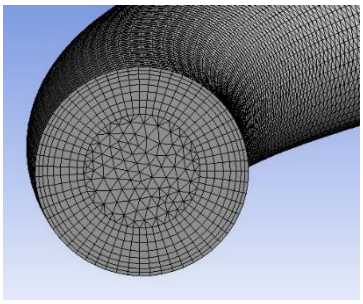

Figure 5. Sample mesh for the CHE.

Boundary Conditions

The boundary conditions include i) no-slip and no-penetration conditions exist on the coil wall, ii) constant temperature and velocity inlet conditions were used in the CHE inlet, iii) the convection heat transfer coefficient and temperature subjected to the CHE surface were determined using the analytical approach presented in the previous section, iv) the turbulence intensity was assumed to be 5% at the inlet.

Numerical Solution

The computational domain was discretized using tetrahedron elements with structured elements in the wall-normal direction. The k–ω turbulence model was used to evaluate the fluid domain of the curved pipe. The coupling of pressure and velocity was made with the SIMPLE algorithm. Second-order upwind schemes were employed for integrating the governing equations with the boundary conditions over the computational domain. The y+ value was ensured ~1 for all simulations to obtain the high resolution of gradients in the near-wall regions. The solution convergence was satisfied when the scaled residuals of continuity, momentum, turbulence kinetic energy, turbulent dissipation rate, and energy ceased after about 800 successive iterations. The values of the scaled

residuals were in the order of less than 10^{-4} for continuity, less than 10^{-5} for velocity components, turbulent kinetic energy, and turbulent dissipation rate and less than 10^{-7} for energy.

EXPERIMENTAL ANALYSIS

An experimental setup was installed for verifying the presented model as shown in Figure 6. The setup basically consists of a temperature-controlled electric heater (TCEH), a cooking pot (CP), water preheating tanks (WPTs), a thermal expansion tank (TET), a gear pump (GP) and measuring instruments. The HTF used in the system was selected to be Renolin therm 320 thermal oil −whose thermo-physical properties given in Eqs. (13)−(16) (Yılmaz and Göksu, 2016; Yılmaz *et al.*, 2017; Yılmaz *et al.*, 2018)− to easily control the process-temperature and make the energy analyses precisely. A frequency-controlled gear pump (Yildizpompa, 2019) was used to adjust the flow rate of the HTF. The outer surface of the CP was insulated with a 40 mm-thick rock wool covered with an aluminum sheet (Izocam, 2019). The TCEH was specially designed heat exchanger (coiled square duct enclosed by an electric heater) which was used to supply thermal power to the HTF. The effective power of the TCEH was 6 kW which was controlled by a PID (Proportional Integral Derivative) controller. When the operating temperature of the system fell below the load-temperature, the TCEH was activated automatically to increase the return-temperature of the HTF to the load-temperature. The role of the WPT was preheating the process-water up to 90 °C. The TET was used to provide additional space for the thermally expanded HTF.

The temperature measurements in the experimental setup were performed by the resistance temperature detectors (Pt100, Class A) connected with two leads (Ordel, 2019). The temperature-dependent uncertainty of the detectors was designated by the relation of $\pm(0.15 + 0.002T)$ °C and calibrated according to the standard of IEC751:1983 (BS EN 60751:1996) by the manufacturer. The surface temperature of the CP was measured from several points using a portable device (Mastech MS8217 with K-type thermocouple) and averaged to use it the analytical model. The operating pressure measurements for the CP were realized by pressure gauges (Pakkens, 2019). In order to measure the pressure at high temperatures, the gauges were connected to the CP by a pigtail siphon. The mass flow rate of the HTF was measured by a Coriolis flow meter having an accuracy of ±0.1% with a repeatability of less than 0.05% (Krohne, 2019). During the experimental tests, the signal data of the measurement devices were collected by the 24-bit USB-2416 and USB-TEMP data acquisition (DAQ) devices for further analyses. For this task, highly-accurate voltage and temperature processing DAQ devices (Mccdaq, 2019a, 2019b) were selected and managed by an interface software program (TracerDAQ Pro) to process data by virtual graphing and data logging.

Figure 6. Experimental setup.

Error Analysis

The uncertainty in experimental measurements describes the factors that are to be taken into consideration such as instrument accuracy etc. A precise method for estimating uncertainty in experimental results has been presented by (Kline and McClintock, 1953).

The surface area of the CHE can be calculated using Eq. (35). Thus, the uncertainty is given by the expression as

$$w_R = \left[\left(\frac{\partial R}{\partial x_1} w_1 \right)^2 + \left(\frac{\partial R}{\partial x_2} w_2 \right)^2 + \cdots + \left(\frac{\partial R}{\partial x_n} w_n \right)^2 \right]^{1/2} \quad (37)$$

where w_R is the standard uncertainty in the result and w_1, w_2, … , w_{x_i} , … w_n are the standard uncertainties of the independent variables.

$$w_{\dot{Q}} = \left[\left(\frac{c_p \left(T_{in} - T_{ex}\right)}{h_i \Delta T_{lm}} w_{\dot{m}} \right)^2 + \left(\frac{\dot{m} \left(T_{in} - T_{ex}\right)}{h_i \Delta T_{lm}} w_{c_p} \right)^2 + \left(\frac{\dot{m} c_p}{h_i \Delta T_{lm}} w_{\Delta T} \right)^2 + \left(-\frac{\dot{m} c_p \left(T_{in} - T_{ex}\right)}{h_i \Delta T_{lm}^2} w_{\Delta T_{lm}} \right)^2 \right]^{1/2} \quad (38)$$

The temperature-dependent error of the temperature detectors is designated by the relation of $\pm(0.15 + 0.002\Delta T)$ °C and calibrated according to the standard of IEC751:1983 by the manufacturer (Ordel, 2019). The temperature-dependent uncertainty for the specific heat capacity of the HTF was included as a function of temperature given in Eq. (14). The flow meter has an accuracy of ±0.1% with a repeatability of less than 0.05%. The USB-TEMP Daq device contributes additional error except the error of the sensor itself. Typically, the maximum error is ± 0.11 °C for the temperature range of 0−150 °C.

Preparation of Materials

For the cooking facility, sample to water ratio of 1:2 was used to satisfy a high degree of starch gelatinization in wheat grains since the transition temperatures for

gelatinization depend on the availability of water (Münzing, 1991). As the moisture levels of starch are reduced, the starch transition temperature increases to higher levels.

The wheat used in the experiments was received from a regional wheat producer as cleaned i.e. separated from dust, foreign materials, and broken wheat. The test results of the wheat properties are given in Table 2. For the statistical analysis, ANOVA was performed for the predicted data to determine the significant differences ($P < 0.05$). Duncan's multiple range tests were carried out. The experiments were replicated and the measurements were duplicated. Note that the mass of the wheat and the corresponding mass of water used in cooking were specified as 13 kg and 26 kg, respectively.

Table 2. Properties of wheat used in experiments.

	Properties	Values	SD (n = 4)
	Type	Hard	–
Color	L^*	51.45	0.0568
Color	a^*	9.6	0.2998
Color	b^*	26.51	0.2968
Color	YI	77.81	0.0734
	Moisture content,	6.00	0.0046
	Protein (% d.b.)	9.01	0.0146
	Ash (% d.b.)	1.48	0.0017
	Specific heat, $c_{p,d}$	1975	25.0545

Table 3. Variation in the grain moisture content.

During preheating						
Initial moisture content (% d.b.)			6.00			
Grain moisture content	°C	T_m	85	90	95	100
	(% d.b.)	12.01	16.07	33.21	37.36	39.33

During boiling			
t (min)	W (% d.b.)	t (min)	W (% d.b.)
5	42.73	30	77.62
10	49.23	35	83.58
15	59.73	40	90.74
20	68.98	45	94.74
25	71.6	50	100.3

The color of the wheat samples was measured by HunterLab Colorimeter (Hunterlab, 2019). The moisture content of wheat was measured at 105 °C using oven method (AOAC, 1990). The Kjeldahl method was used to determine the protein contents of wheat using the methodology presented in (AOAC, 1990). The ash contents of wheat were measured at 900 °C according to (AOAC, 1990). The specific heat of the dry wheat grains was measured by using energy balance applied in Eq. (1). Additionally, the variation in grain moisture content during preheating and boiling processes was measured as indicated in Table 3. This dataset is significant to predict the specific heat of wheat grains during preheating and the time period of cooking process for complete gelatinization. The measurement procedure for this dataset is as follows: grain samples were extracted from the CP (open to the atmosphere) at each 5 °C temperature-interval during the preheating process. Through the boiling process, grain samples were taken out of each 5-min time interval and then quenched in cold water. After removing the surface moisture, grains were wrapped and sheltered at 4 °C to prevent moisture loss before measuring the moisture content of grains for each batch.

Each cooking process was operated in a total time period of 50 min of which 5 min time period was specified to be the resting for boiled wheat grains and the complete discharging of the vapor inside the CP at the end of the cooking process. During the cooking operation, the boiled water was directed to a double pipe heat exchanger connected to the pressure relief valve. It was designed for condensing the water with an effective heat transfer area of 5×10^{-2} m^2. The water being boiled was cooled by the water circulating through the double pipe heat exchanger. At the end of the cooking operation, the total condensed water was measured by a sensitive balance. Thus, the amount of heat rejected or the boiling loss was basically estimated for the entire cooking process:

$$Q_r = m_v h_{fg} = m_w c_{p,w}\left(T_p - T_w\right) \tag{39}$$

RESULTS AND DISCUSSION

The results of the developed thermal model were compared with those of the numerical model and the experiments. The model outputs for the CP were obtained for different cooking parameters given in Table 4. It is seen that the model yields pretty good results for the prediction of the heat transfer area of the CHE and the exit temperature of the HTF even at saturation (i.e. boiling) temperature higher than 100 °C. This validation is very significant for describing the most effective parameters of the cooking process in terms of energy efficiency. Besides, it can be useful in the design stage of large-scale CPs and their efficient energy control.

Figure 7 shows the results obtained from the experimental analyses and the numerical and thermal models. The numerical and analytical results were compared with the experimental results and good agreement was obtained. While the maximum deviation of the outlet temperature is 1.12% for the numerical analysis, it is around 0.38% for the analytical approach.

Although the thermal model provides the advantage of solution simplicity, it gives limited information about the flow properties of HTF but is sufficient to make a CP design. On the contrary, making a numerical analysis is tedious and time-consuming; it provides better insight into fluid dynamics properties. The developed thermal model which estimates the outlet temperature of the designed CHE favorably will ensure to calculate the energy transferred to the mixture in the CP. This knowledge is significant both in the stage of CP design, energy optimization and system control. In Turkey, all CP producers make their designs using trial and error or by experience. However, this does not constantly give satisfying results when the CP capacity and the operating

Table 4. Predictions of the analytical model for sample experiments.

Experimental								Model						
N	$\dot{m}_{htf}$	T_{in}	T_{ex}	T_{sat}	T_{ins}	T_{air}	Δt_2	h_i	Re	h_o	T_s	T_{ex}	A_s	Uncertainty
–	kg/s	°C	°C	°C	°C	°C	sec	W/m²°C	–	W/m²°C	°C	°C	m²	A_s , %
1	0.0847	150.0	132.4	100.0	52.1	40.0	2,700	360	3184	2,371	105.4	132.6	0.290	1.93
2	0.0916	145.0	129.8	100.1	52.3	39.5	2,700	377	3253	2,265	105.4	129.8	0.289	2.17
3	0.1000	140.0	127.0	100.2	53.7	37.1	2,700	397	3341	2,152	105.3	127.0	0.287	2.48
4	0.1111	135.0	124.5	100.0	53.5	37.7	2,700	424	3494	1,995	104.9	124.0	0.272	2.96
5	0.1378	130.1	121.5	100.0	53.6	37.2	2,700	494	4060	1,996	104.9	121.3	0.279	3.55
6	0.1380	122.6	116.4	100.1	53.1	37.8	2,700	478	3642	1,597	104.4	116.4	0.286	4.81
7	0.1904	130.9	125.4	110.2	56.2	36.0	2,220	674	5835	2,070	114.5	125.3	0.280	5.33
8	0.2258	130.8	128.2	120.2	56.0	36.2	1,400	805	7072	1,564	123.4	128.3	0.299	10.99

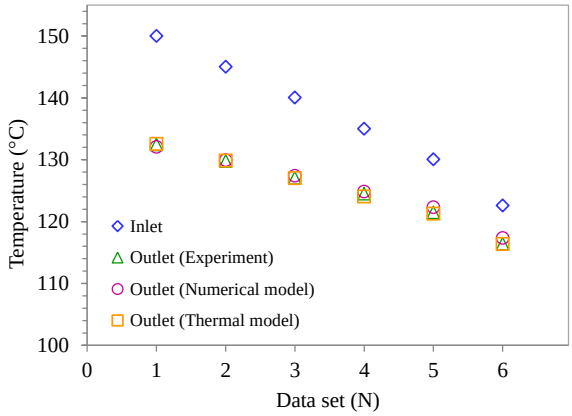

Figure 7. Comparison between the theories and practice.

conditions change. Moreover, this would not result in energy-efficient CP and lead to having a systematic approach for waste heat recovery. When the system parameters vary with design or operation, the system control would not able to sustain energy optimization anymore. For this reason, the developed models will provide benefits from various aspects.

Temperature contours at the outlet of the CHE are illustrated in Figure 8 for each case given in Figure 7. The flow pattern is quite different relative to a straight tube since the most prominent characteristic of flow in helicoidal pipes is the secondary flow induced by centrifugal force which causes the fluid particles inner side of the CHE to move faster than the outer and thus provides benefit to enhance the heat transfer rate. The degree of secondary flow lowers gradually as moving from Figure 8a to 8f. This is related to the balance between the inlet temperature of the CHE and the corresponding mass flow rate of the HTF demanded by the cooking process. As the inlet temperature increases, the mass flow rate is reduced to adjust the sufficient heat load that needs to be transferred to the mixture in the CP. At high inlet temperatures, the average HTF velocity is relatively low thus it is probably earlier the secondary flow at the pipe outlet to develop. This means that increasing the HTF velocity in the CHE results in less chance to develop the secondary flow. Therefore, the inlet temperature, HTF properties and velocity, and pipe length are important design parameters that need to be specified properly so that the convection heat transfer coefficient in the CHE is enhanced.

During the cooking process, the minimization of the thermal energy supply accompanied by preserving the final product quality is essential and can be improved. The heat flux transferred to the mixture, $\dot{q}_b$ should be adjusted as initiating the ONB since bubbles during nucleate boiling serve as energy movers and provide upside-down movement of the mixture. Bayram (2006) also proposed that the cooking temperature is to be at boiling temperature to benefit from the mixing effect of water bubbles. Thus, the regime of boiling is a decisive parameter for enhancing the convective heat transfer coefficient and effective cooking. Increasing the convection heat transfer coefficient will increase the mass transfer to wheat kernels and quicken the gelatinization. However, as the ONB point is over exceeded, the boiling loss and accordingly the energy consumption will increase. Furthermore, the disruption of wheat kernels and leaching of the starch during cooking operation are affected by the strength of nucleate bubbles. This may cause lots of problems such as stickiness, size deformation, nutrient loss, etc. (Bayram *et al.*, 2004). Using a mechanical mixer inside the CP can satisfy homogeneous mixing and cooking enhancement but this will cause deformation of wheat grains. Therefore, cooking conditions should be well arranged for product quality to ensure complete gelatinization without deforming, darkening and making the product so, sticky. On the other hand, increasing the heat flux on the CHE strengthens the boiling which, in turn, increases the organic and coloring compounds leached into the water and changes the watercolor to dark. Additionally as the level of the leaching intensifies, the water becomes much denser and its viscosity increases during boiling due to water absorption by the wheat grains and water unavailability with time. This partially prevents the bubble movements and causes to lessen nucleate mixing toward the end of the cooking process. Thus, it is supplied more energy to the mixture in practical applications for this problem to obtain complete gelatinization at the bottom side (conical part) of the CP An increasing mass of wheat grains at the upper part

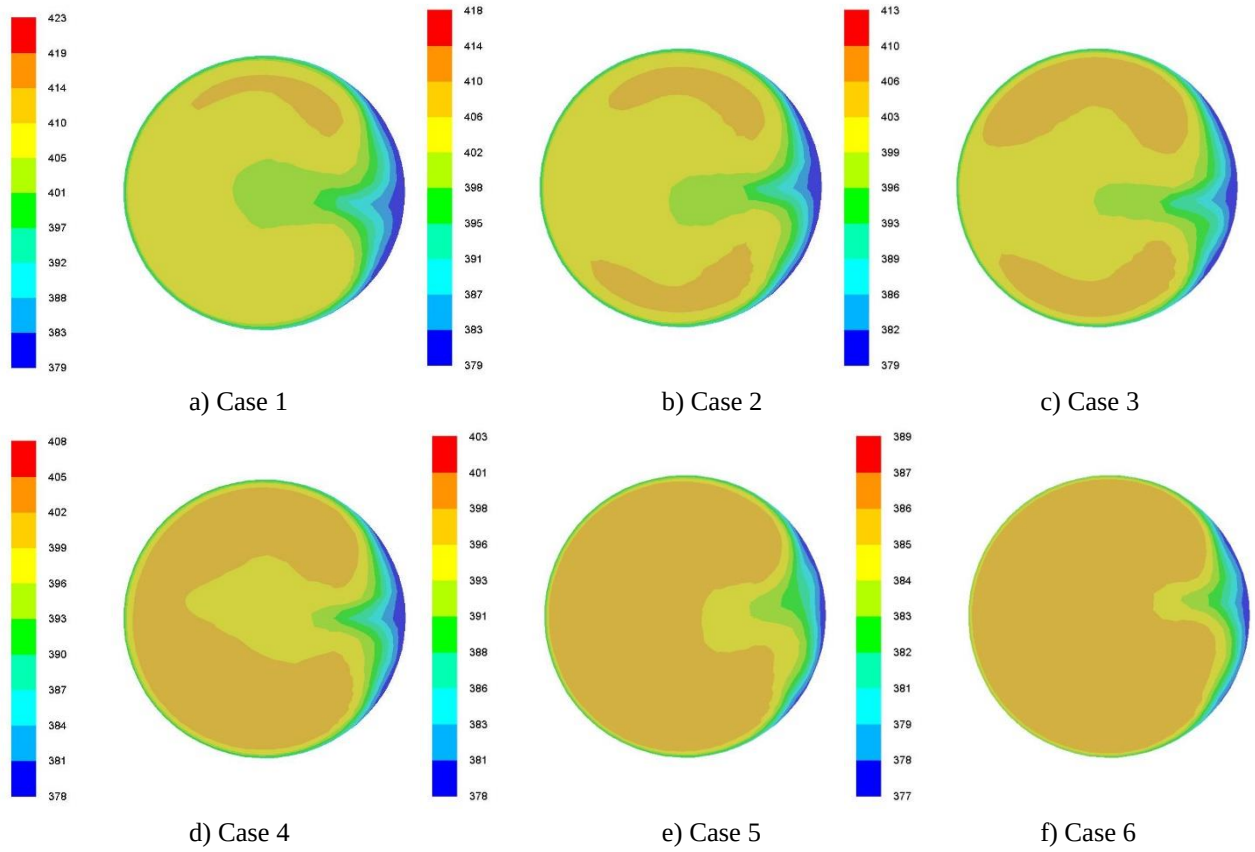

a) Case 1 b) Case 2 c) Case 3

d) Case 4 e) Case 5 f) Case 6

Figure 8. Temperature contours at the CHE outlet (as Kelvin) for the specified cases.

makes cushion effect to the bottom or applies pressure which degrades the gelatinization of grains in that region. Another factor causing ineffective energy transfer to that part is the reduced HTF temperature at the downstream of the CHE. Thus, the minimization of the energy consumption results in many problems which should be considered thoroughly.

Table 5 shows the cooking parameters of boiled wheat obtained from different batches. The results reveal that the inner structure of wheat grains, their initial moisture content and thermo-physical properties affect cooking quality and cooking time for complete gelatinization. The complete gelatinization depends strongly on wheat properties, cooking time, boiling temperature and regime. Water absorption of wheat samples (i.e., moisture uptake) during the cooking process can give information about the level of gelatinization. The minimum moisture content of boiled wheat on dry basis (d.b.) must be at the level of 100%. In this study, the cutting method to examine the gelatinization was used where 100 cooked kernels were cut into two equal pieces and then the endosperms were examined for the opaque white center. As seen from Table 5, the yellowness index is inversely affected by increasing the boiling temperature but this is not desired for the final product quality. For the calculation of BOD_5, the method presented by Balcı and Bayram (2020) was used. Most of the BOD_5 values are lower than half of the results presented by Balcı and Bayram (2020) who obtained 429.5 mg/L under controlled experimental conditions. One of the followed methods in this study is the minimization of energy demand for cooking which results in reduced BOD_5 values due to decreasing leaching substances with reducing energy supply during the boiling process. Wastewater of a bulgur plant is disposed to the environment however it has a high value of BOD_5 (about 450 mg/L Balcı and Bayram (2020)) which can lead to environmental diseases.

Minimization of the energy need to obtain gelatinized wheat was also investigated in this study. The minimum energy transfer to the mixture was adjusted by keeping the central region of the CP at the boiling temperature. This was accomplished by simultaneously monitoring the measured temperature of the central region on the DAQ interface program and adjusting the flow rate of the HTF using a frequency-controlled pump. The diffusion of convective currents from the CHE to the central part of the CP was effective on this phenomenon. For this reason, the heat flux on the CHE was regulated enough to initiate the nucleate boiling. However, the ONB depends on the fluid–heating material combination and the fluid pressure. Thus, the ONB point specified in Figure 3 is able to change with operating conditions. There is no available correlation in the literature to estimate the ONB point for different combinations. In this study, $\dot{q}_b$ and ΔT_{excess} were calculated and the results presented in Table 4 were obtained. The measurements and the calculations showed that $\dot{q}_b$ ranged from 7,000 W/m^2 to 10,000 W/m^2 at $\Delta T_{excess} \approx 5$ °C. This range is in accord with the region of nucleate boiling presented in Figure 3. Lowering the $\dot{q}_b$ more causes to lessen the bubble density and mixing effect, particularly in large-scale industrial CPs.

Table 5. Properties of wheat for sample cooking operations.

Sample	T_b	Color				Protein	Ash	BOD_5	W
	°C	L^*	a^*	b^*	YI	% d.b.	% d.b.	mg/L	% d.b.
1	100	51.50	8.88	31.78	85.43	10.94	1.26	215.0	103.3
2	100	50.36	8.55	30.49	83.99	10.40	1.32	212.5	108.7
3	100	51.33	9.22	30.39	86.51	10.85	1.32	222.7	114.0
4	100	51.09	8.85	31.71	85.64	11.57	1.21	220.5	108.3
5	100	50.71	9.06	31.96	84.83	11.03	1.22	182.5	103.7
6	100	50.73	9.15	31.36	85.59	10.65	1.25	200.2	104.3
7	110	52.98	7.00	26.40	72.95	9.52	1.58	228.0	100.8
8	110	53.44	7.32	30.99	80.15	9.13	1.08	197.5	98.5
9	120	52.60	7.59	30.27	80.50	9.48	1.10	194.7	101.2
10	120	50.39	7.46	28.00	77.22	10.37	1.24	216.3	111.0

Conventional bulgur plants have operated CPs supplying high energy to wheat grains in order to gelatinize them as much as possible. The cooking state is controlled by the use of centre cutting method, the color of evaporated water from the CP or smell of this water (Bayram, 2006). These simple methods are useful to be able to control the cooking operation during bulgur production due to low labor however these sensory methods are not developed and rely on experience and qualified staff. Recently, this step has left its place to new automated CPs in modern bulgur plants.

In the automated CP, preheating temperature/time, cooking temperature/time, water amount, resting and discharging times are adjusted by the operator who makes these data entry to the control panel of the CP. The energy demand for industrial cooking is supplied indirectly by a steam generator which is generally operated under certain temperature levels and specified thermal loads. The cooking load is adjusted by an operator who manipulates the cooking time until the gelatinization of the grains' structure is maintained. However, this procedure requires operational experience based on the variation in the operational parameters mentioned above. Noting that the properties of raw material and the mixing of the reddish wheat with durum wheat during harvesting and storing also affect the cooking process and final product since finding pure or homogeneous raw material is nearly impossible for bulgur production in undeveloped and developing countries (Bayram and Öner, 2006). Thus, the energy supplied to the mixture in the CP is adjusted by an experienced operator who observes the cooking degree of bulgur at the end of the cooking process. During the cooking process, the geometry of the CP (shape, capacity, etc.) and the properties of the heating element affect the cooking quality. For example, the latest automated CP consumes 1.5 tons of saturated steam at 4.5–5 bar gauge pressure with a steam trap for the cooking process utilizing 5:4 of tons wheat to water ratio. The double-stage cooking operation is used in this system. The CP in the first-stage preheats the water-wheat mixture to a preset temperature of 80–85 °C. The heating element is composed of a CHE in which steam is used. After preheating, the mixture is unloaded into the second-stage which cooks the wheat grains about 25–28 min until the preheating temperature reaches the maximum temperature of 108 °C at the end of cooking. Then, the mixture in this stage is rested about 15 min. The moisture content of the wheat grains reaches 50–52% w.b. (wet basis) at the end of the cooking process. The residual water amount changes between 1–1.2 tons for such a process. The CP in the second-stage has two individual CHEs to enhance the degree of cooking. One of them is used for heating the upper region (cylindrical in shape) of the CP and the other is used for the conical part heating. The use of single-piece CHE requires much energy to keep the HTF temperature at the conical part not lower. Lowering of the steam temperature will lead to ineffective heat transfer at this part of the CP. Moreover, circulation pumps are used to circulate the process-water from the bottom side to the upper. The steam expelled out during the cooking process is used in the first stage of the cooking system for energy efficiency. As a result, the average rate of specific energy consumption is estimated at around 400–500 W/kg (thermal power supplied for one kilogram of wheat) for a modern industrial bulgur plant to produce bulgur. This rate would increase to 800 W/kg for conventional bulgur plants having a single-stage non-automated CP.

Table 6. Water balance for sample cooking operations*.

Sample	m_{ev}	$m_b - m_c$	m_f	m_{loss}	m_r	m_l	m_a	m_t
1	3	903	483	518	12,460	137	11,770	26,000
2	3	1,501	447	565	12,150	140	11,474	26,000
3	3	1,626	406	530	12,200	134	11,369	26,000
4	3	2,001	525	648	11,965	122	10,980	26,000
5	3	2,014	511	583	12,240	124	10,773	26,000
6	3	3,500	436	645	10,453	145	11,108	26,000

*All units in gram.

The experimental findings show that the minimum rate of specific energy consumption is around 325−375 ±5% W/kg in case of preheating the process-water with boiling losses, but it could reach 400−475 ±5% W/kg without using waste heat. When the wheat to water ratio is reduced to 1, the energy supply for preheating could be reduced ~25%. As concluded, the energy need in large-scale CPs can be improved by enhancing the overall convection heat transfer coefficient inside the CP and by lowering the water amount. However, even the energy demand can be reduced as a result of the mentioned improvements; it cannot be lowered any more. Since the average Re in the CHE must be higher than 2,300. Under most practical conditions, the flow in a pipe is laminar for Re < 2,300 which results in low $\dot{q}_b$ to reject heat for a certain pipe length. Otherwise, the pipe length extends too much and it becomes unsuitable for CP design. A conservative approach for fully turbulent is taken as Re > 4,000 in many cases (Çengel and Ghajar, 2011). Thus, the mass flow rate through the CHE is adjusted based on this critical value and the coil length is specified as a function of convection heat transfer coefficient and critical heat flux. Besides, as the coil radius is increased in large-scale applications, the effect of coil curvature on flow decreases and thus the domination of centrifugal forces will be lesser (Jayakumar *et al.*, 2010). In other words, the curved pipe would behave a straight pipe which, in turn, lowers the convection heat transfer coefficient inside the CHE.

The mass balance of water during the cooking process is considered to be significant for energy consumption. Table 6 shows the mass balance for the water utilized during the cooking process. In many conventional bulgur plants, the process-water amount is used 1.4 times of the wheat amount. As a rule of thumb, ~43% of the process-water is absorbed by wheat kernels at the end of the cooking process and ~28% of the process-water is rejected as wastewater and 2.5% of the cooked wheat amount is leached into the wastewater in industrial practices. The water uptake (m_a) calculated in this study is coherent with the industrial data and the wastewater amount (m_r) is higher relative to the practice since the energy optimization has yielded lower water evaporation. It is noted that 1.4-ratio corresponds to 2.0-ratio in our experimental study. Based on 2.0-ratio, the percentage of wastewater will increase from 28% to 40%. While m_r obtained from this study was around 12,000 gr, it would have been ~10,400 gr (26,000×40%) based on the data of industrial practice. Sample 2 in Table 6 shows that the wastewater amount is close to the practice since the energy supplied to the mixture was high and more water was accordingly evaporated during boiling. The total amount of leached substances was measured by evaporating the sample residual water. The percentage of leached substance was about half of the industrial practice which is pretty consistent with the practice since BOD_5 which is a measure of leached substance amount in the wastewater was reduced to less than half as compared to the practice.

At the end of the cooking process, the butterfly valve of the CP is opened and the residual water is discharged into a collecting vessel. Some part of this water which flashed and evaporated into ambient air constitutes ~4% of the process-water amount. The amount of water flashed depends strongly on atmospheric conditions such as atmospheric pressure, the relative humidity of a location. The instantly measured values by the Turkish State Meteorological Service (MGM, 2019) were used in the calculations. As seen, the estimated m_{ev} values are negligible to consider it in the water balance.

CONCLUSION

Turkey is the biggest bulgur producer (1,230,766 tons per annum as of 2018 (TMO, 2019)) in the world and exports annually above 120 million $ to other countries. In Turkey, there are a great number of manufacturers producing CPs at different types and performance. The designs of these systems are generally made by trial and error or experience however this is not an effective method of getting these systems better without prior theoretical analyses. This study presents the details of the wheat cooking process and a novel thermal model for designing CP (having CHE as an energy supplier or heating element) which is widely used in bulgur plants. The effect of the heating element and its design properties have been discussed from the views of energy efficiency and bulgur quality. The findings of this study which would guide CP producers and bulgur plants positively are as follows:

- The ONB serves as an energy mover and provides upside-down movement of the mixture via nucleate bubbles. It depends upon the critical heat flux on the CHE which corresponds to $\Delta T_{excess} \approx 5$ °C. This value is significant to estimate the critical heat flux and the surface area of the CHE for regulating energy efficiency. Increasing the critical heat flux which, in turn, causes more water to be evaporated during cooking increases the water unavailability in the CP. As a result, this may result in producing ungelatinized wheat kernels if wheat to water ratio is around 1.
- Changing the coil pitch has a negligible effect on the Nu inside the CHE whereas the effect of coil radius decreases it. Increasing the diameter of the coil requires having a lengthy pipe to attain a fully developed flow. The proper sizing of CHE is very essential for both the volume in the CP and the heat transfer properties of flow to accomplish the task.
- The minimum energy supplied to the mixture is related to the degree of wheat kernels being completely gelatinized at the end of the cooking process. This can be performed by accelerating the nucleate bubble formations, i.e. initiating the nucleate boiling. Only supplying energy during the cooking process to meet the heat loss of the CP does not accomplish the complete gelatinization and extends the gelatinization time since the diffusion of

water into starch is related to the enhancement of boiling convection heat transfer coefficient.

- The estimated average rate of specific energy consumption lies between 400–500 W/kg (thermal power supplied for one kilogram of wheat) for a modern industrial bulgur plant whereas it would increase to 800 W/kg for conventional bulgur plants having single-stage CP. The experimental findings have indicated that the corresponding range could be between 325–375 ±5% W/kg with waste heat recovery (otherwise it would reach to 400−475 ±5% W/kg) and doubled process-water amount. The estimated range can be reduced both by reducing the water amount (this minimizes only the energy consumption through the preheating of the mixture ~25%) and enhancing the convection heat transfer coefficient of the HTF inside the CHE using steam instead of thermal oil.
- The minimization of energy supply for cooking has a positive effect on BOD_5. BOD_5 which is about 450 mg/L in the wastewater of a bulgur plant has been reduced less than half of that value by the energy optimization strategies.
- The process-water can be reduced to half by water recovery, i.e. decreasing wheat to water ratio to 1:1−1:1.2 as the study clearly indicates. This knowledge is also supported based on the applications of a modern bulgur plant. Reducing water amount will have a positive effect on the energy demand minimization.
- Insulating the outer side of the CP is essential to minimize the heat loss to the surroundings up to 3–4 based on the operating conditions. As seen in Table 4, the insulation material prevents the CP outer surface to increase higher levels i.e. boiling temperature. This is not a common application in Turkish bulgur plants. The inclination angle of the cover plate is to be adjusted lower than 20° if the evaporated water is used in the second stage of the CP and it would be higher than 20° if the evaporated water is to be condensed in the CP. The latter case benefits water recovery. A non-insulated cover plate of the CP will also cause to increase the condensation on the plate.

ACKNOWLEDGEMENT

This study was funded by the Scientific Research Projects Governing Unit of Gaziantep University with grant no. MF.11.13. Authors also appreciate Dr. Fatih Balcı (Food Engineer), Günmak Milling Machinery Co. (Manufacturer of cooking and drying systems for bulgur) and Arbel Group (Making production and processing of bulgur) for their cooperation in part of the study. Any opinions, findings and conclusions or recommendations expressed in this study are those of the authors and do not necessarily reflect the views of the cooperators.

REFERENCES

AOAC, 1990, *Official Methods of Analysis of the Association of Official Analytical Chemists*, (Fifteenth Ed.), Washigton, DC.

Bakshi A. S. and Singh R. P., 1980, Kinetics of water diffusion and starch gelatinization during rice parboiling, *J. Food Sci.*, 45(5), 1387-1392.

Balcı F. and Bayram M., 2020, Bulgur cooking process: Recovery of energy and wastewater, *J. Food Eng.*, 269, 109734.

Bayram M., 2005, Modelling of cooking of wheat to produce bulgur, *J. Food Eng.*, 71(2), 179-186.

Bayram M., 2006, Determination of the cooking degree for bulgur production using amylose/iodine, centre cutting and light scattering methods, *Food Control*, 17(5), 331-335.

Bayram M. and Öner M. D., 2006, Determination of applicability and effects of colour sorting system in bulgur production line, *J. Food Eng.*, 74(2), 232-239.

Bayram M., Öner M. D. and Eren S., 2004, Effect of cooking time and temperature on the dimensions and crease of the wheat kernel during bulgur production, *J. Food Eng.*, 64(1), 43-51.

Bruce D. and Giner S., 1993, Mathematical modelling of grain drying in counter-flow beds: investigation of crossover of air and grain temperatures, *J. Agr. Eng. Res.*, 55(2), 143-161.

Chin Y.-S. S., 1995, *Numerical solution of the complete two-phase model for laminar film condensation with a noncondensable gas*, Ph.D. Thesis, Manitoba University, Canada.

Churchill S. W. and Chu H. H., 1975, Correlating equations for laminar and turbulent free convection from a vertical plate, *Int. J. Heat Mass Tran.*, 18(11), 1323-1329.

Cornwell K. and Houston S., 1994, Nucleate pool boiling on horizontal tubes: a convection-based correlation, *Int. J. Heat Mass Tran.*, 37, 303-309.

Çengel Y. A. and Ghajar A. J., 2011, *Heat and mass transfer: Fundamentals & Applications* (Fourth Ed.), McGraw-Hill, New York.

Fuchs, 2013, Opet Fuchs Mineral Oil Industry and Trade Inc., Izmir, Turkey, *Renolin Therm 320 Product Information*.

Fujii T. and Imura H., 1972, Natural-convection heat transfer from a plate with arbitrary inclination, *Int. J. Heat Mass Tran.*, 15(4), 755-767.

Gerstmann J. and Griffith P., 1967, Laminar film condensation on the underside of horizontal and inclined surfaces, *Int. J. Heat Mass Tran.*, 10(5), 567-580.

Hogg G. W., 1969, *The effect of secondary flow on point heat transfer coefficients for turbulent flow inside curved tubes*, Ph.D. Thesis, Idaho University, Moscow.

Hunterlab, 2019, *Colorflex specifications*, https://www.hunterlab.com/colorflex-ez-specifications.pdf.

Izocam, 2019, *Technical datasheet of Izocam industrial blanket*, http://www.izocam.com.tr/p157-industrial-blanket.html.

Jayakumar J., Mahajani S., Mandal J., Iyer K. N. and Vijayan P., 2010, CFD analysis of single-phase flows inside helically coiled tubes, *Comput. Chem. Eng.*, 34(4), 430-446.

Kline S. and McClintock F., 1953, Describing uncertainties in single-sample experiments, *ASME Mech. Eng.*,75(1), 3-8.

Koca A. F. and Anıl M., 1996, Farklı buğday çeşitleri ve pişirme yöntemlerinin bulgur kalitesine etkisi, *Gıda Dergisi*, 21(5).

Krohne, 2019, *Optimass 6000 technical datasheet*, https://cdn.krohne.com/fileadmin/media-lounge/files-marine/Downloads_pdf/TD_OPTIMASS_6000.pdf.

Manlapaz R. L. and Churchill S. W., 1981, Fully developed laminar convection from a helical coil, *Chem. Eng. Commun.*, 9(1-6), 185-200.

Marrero T. R. and Mason E. A., 1972, Gaseous diffusion coefficients, *J. Phy. Chem. Ref. Data*, 1(1), 113-118.

Mccdaq, 2019a, *USB-2416 User's Guide*, https://www.mccdaq.com/pdfs/manuals/USB-2416.pdf.

Mccdaq, 2019b, *USB-TEMP User's Guide*, https://www.mccdaq.com/pdfs/manuals/USB-TEMP.pdf.

MGM, 2019, *Weather forecast for Gaziantep*, https://www.mgm.gov.tr/tahmin/il-ve-ilceler.aspx?il=Gaziantep&ilce=%C5%9Eehitkamil.

Minkowycz W. and Sparrow E., 1966, Condensation heat transfer in the presence of noncondensables, interfacial resistance, superheating, variable properties, and diffusion, *Int. J. Heat Mass Tran.*, 9(10), 1125-1144.

Münzing K., 1991, DSC studies of starch in cereal and cereal products, *Thermochim. Acta*, 193, 441-448.

Mwesigye A., Yılmaz İ. H. and Meyer J. P., 2018, Numerical analysis of the thermal and thermodynamic performance of a parabolic trough solar collector using SWCNTs-Therminol® VP-1 nanofluid, *Renew. Energ.*, 119, 844-862.

Ordel, 2019, *Resistance thermometer*, http://www.ordel.com.tr/en/urun/or60.

Orlov V. and Tselishchev P., 1964, Heat exchange in spiral coils with turbulent flow of water, *Therm. Eng. (*Translated from Teploenergetika*)*, 11(12), 97.

Pakkens, 2019, *Accurate pressure gauges*, http://www.pakkens.com.tr/products/basinc-olcerler-1/hassas-manometre-6/?lang=en.

Pratt N. H., 1947, The heat transfer in a reaction tank cooled by means of a coil, *T. I. Chem. Eng.-Lond.*, 25, 163-180.

Rocca-Poliméni R., Flick D. and Vasseur J., 2011, A model of heat and mass transfer inside a pressure cooker, *J. Food Eng.*, 107(3-4), 393-404.

Rohsenow W. M., Hartnett J. P. and Cho Y. I., 1998, *Handbook of Heat Transfer* (Third Ed.), McGraw-Hill, New York.

Srinivasan P., Nandapurkar S. and Holland F., 1970, Friction factors for coils, *Trans. Inst. Chem. Eng.*, 48(4-6), T156-T161.

Stapley A., Fryer P. and Gladden L., 1998, Diffusion and reaction in whole wheat grains during boiling, *AICHE J.*, 44(8), 1777-1789.

TMO, 2019, *Turkish grain board*, http://www.tmo.gov.tr/Upload/Document/hububatsektor raporu2018.pdf.

Turhan M. and Gunasekaran S., 2002, Kinetics of in situ and in vitro gelatinization of hard and soft wheat starches during cooking in water, *J. Food Eng.*, 52(1), 1-7.

Watanabe H., Fukuoka M., Tomiya A. and Mihori T., 2001, A new non-Fickian diffusion model for water migration in starchy food during cooking, *J. Food Eng.*, 49(1), 1-6.

Yildizpompa, 2019, *Technical properties of YKF-1" internal eccentric gear pump*, http://www.yildizpompa.com/wp-content/uploads/2017/11/YKF-1%C2%BD.pdf.

Yılmaz İ. H. and Söylemez M. S., 2014, Thermo-mathematical modeling of parabolic trough collector. *Energ. Convers. Manage.*, 88, 768-784.

Yılmaz İ. H., 2014, *A theoretical and experimental study on solar-assisted cooking system to produce bulgur by using parabolic trough solar collector*, Ph.D. Thesis, Gaziantep University, Turkey.

Yılmaz İ. H., 2018, *Energy efficient cooking pot* (In Turkish: Enerji verimli pişirme kazanı), Patent No: TR 2015 13024 B, Turkish Patent and Trademark Office. Turkey.

Yılmaz İ. H. and Göksu T. T., 2016, Experimental and CFD analyses of a helicoidal heat exchanger, *International Energy Engineering Congress 2016*, Gaziantep, Turkey, 638-646.

Yılmaz İ. H., Göksu T. T., Kılıç M. and Söylemez M. S., 2017, Performance comparison of circular and square cross-sectioned helicoidal heat exchangers using experimental and CFD analyses, *International Conference on Advances and Innovations in Engineering*, Elazıg, Turkey, 487-490.

Yılmaz İ. H., Hayta H., Yumrutaş R. and Söylemez M. S., 2018, Performance testing of a parabolic trough collector array for a small-scale process heat application, *ISI BILIM TEK DERG* (Journal of Thermal Science and Technology), 38(1), 43-53.

Yılmaz İ. H. and Mwesigye A., 2018, Modeling, simulation and performance analysis of parabolic trough solar collectors: A comprehensive review, *Appl. Energ.*, 225, 135-174.

İbrahim Halil YILMAZ is an associate professor at the Mechanical Engineering Department of AAT Science and Technology University, Adana, Turkey. He received his B.Sc. (2005), M.Sc. (2009) and Ph.D. (2014) degrees in Mechanical Engineering Department of Gaziantep University. He worked in several positions including Gaziantep University (2007−2016), Zurich Technopark (2009), and German recycling sector (2009). He is the author or co-author of more than 50 scientific papers in the international prestigious journals or conferences. His main research interests include green energy systems, thermal system design and modeling, analytical and numerical heat transfer/fluid flow, refrigeration systems, biomass to power, and machine learning for renewables.

Mehmet Sait SÖYLEMEZ is a professor at the Mechanical Engineering Department of Gaziantep University, Gaziantep, Turkey. He obtained his B.Sc. (1985) and M.Sc. (1988) degrees from the Mechanical Engineering Department of Middle East Technical University, and his Ph.D. (1992) in the Mechanical Engineering Department of Gaziantep University. He has published more than 50 scientific papers in various international journals and conferences. His main research areas are refrigeration, heat pumps, solar energy, heat transfer and thermo-economic optimization.